

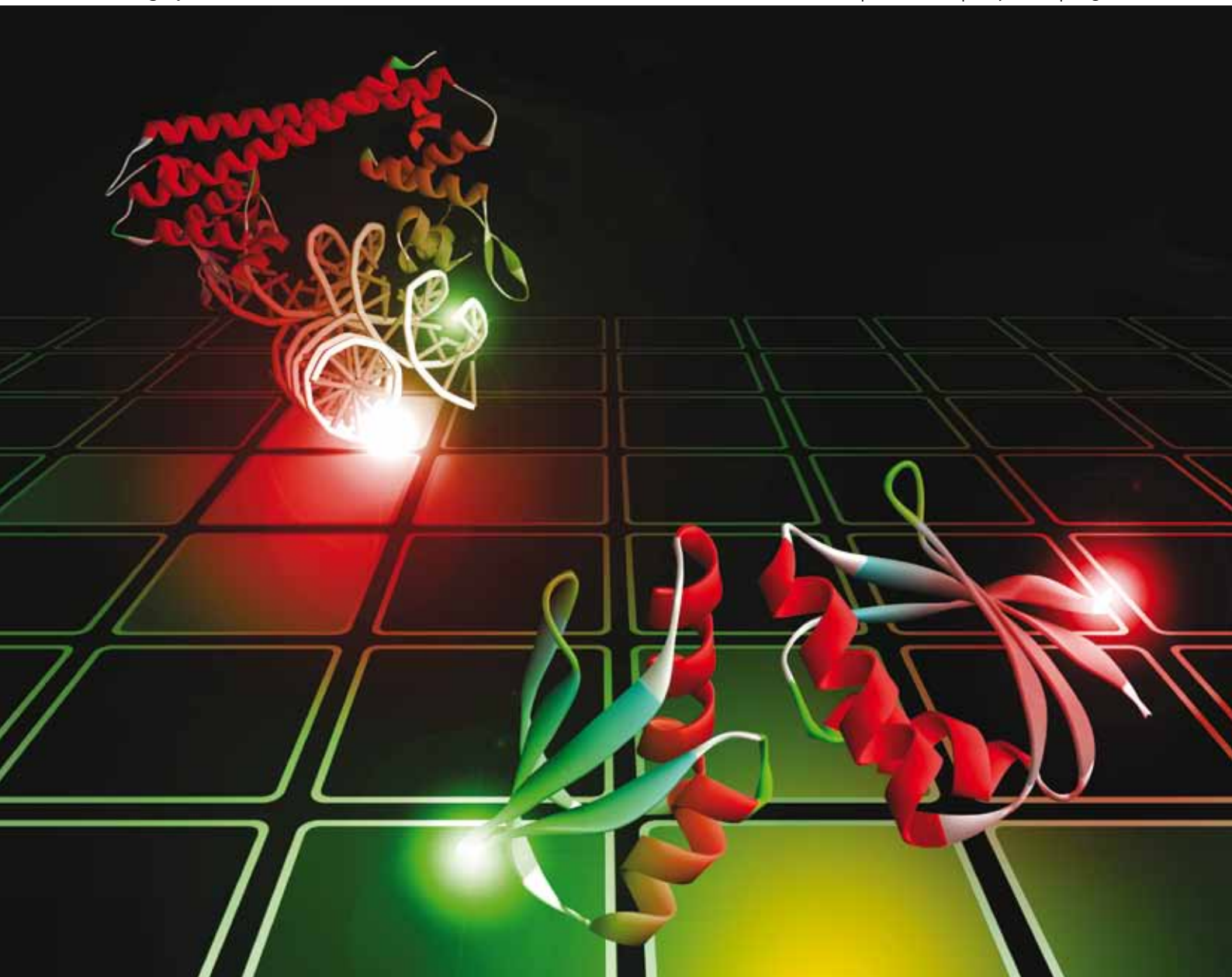
NPR

Natural Product Reports

Current developments in natural products chemistry

www.rsc.org/npr

Volume 27 | Number 5 | May 2010 | Pages 625–796



Themed issue: Metals in cells

ISSN 0265-0568

RSC Publishing

REVIEW

Peng Chen *et al.*

Tackling metal regulation and transport at the single-molecule level



0265-0568(2010)27:5;1-8

Tackling metal regulation and transport at the single-molecule level†

Peng Chen,* Nesha May Andoy, Jaime J. Benítez, Aaron M. Keller, Debashis Panda and Feng Gao

Received 1st December 2009

First published as an Advance Article on the web 5th March 2010

DOI: 10.1039/b906691h

Covering: up to 2009

To maintain normal metal metabolism, organisms utilize dynamic cooperation of many biomacromolecules for regulating metal ion concentrations and bioavailability. How these biomacromolecules work together to achieve their functions is largely unclear. For example, how do metalloregulators and DNA interact dynamically to control gene expression to maintain healthy cellular metal level? And how do metal transporters collaborate dynamically to deliver metal ions? Here we review recent advances in studying the dynamic interactions of macromolecular machineries for metal regulation and transport at the single-molecule level: (1) The development of engineered DNA Holliday junctions as single-molecule reporters for metalloregulator–DNA interactions, focusing on MerR-family regulators. And (2) The development of nanovesicle trapping coupled with single-molecule fluorescence resonance energy transfer (smFRET) for studying weak, transient interactions between the copper chaperone Hah1 and the Wilson disease protein. We describe the methodologies, the information content of the single-molecule results, and the insights into the biological functions of the involved biomacromolecules for metal regulation and transport. We also discuss remaining challenges from our perspective.

- 1 Introduction
- 2 Metal-sensing transcriptional regulation
 - 2.1 MerR-family metalloregulators: protein–DNA interactions of subtle structural changes as a challenge
 - 2.2 Methodology: engineered DNA Holliday junctions as smFRET reporters for protein–DNA interactions
 - 2.3 Application to interactions of PbrR691 and CueR with DNA
- 3 Intracellular copper transport
 - 3.1 Copper chaperones: weak, dynamic protein interactions as a challenge
 - 3.2 Methodology: nanovesicle trapping combined with smFRET
 - 3.3 Application to interactions between the copper chaperone Hah1 and the Wilson disease protein
- 4 Remaining challenges
 - 4.1 Metalloregulators
 - 4.2 Metallochaperones
- 5 Acknowledgements
- 6 References

1 Introduction

Metals are essential for life processes, including oxygen transport, electron transport, and neurological signaling.¹ However,

they can also be toxic, especially at high concentrations. To have normal metabolism, organisms tightly regulate the intracellular concentrations and bioavailability of metal ions.^{2–4}

A variety of protein machineries contribute to intracellular metal homeostasis. Membrane metal transporters control metal ion uptake into and efflux out of the cell (Fig. 1A, B).^{2,5,6} Inside cells, metalloregulators sense metal ion concentrations and regulate the transcription of genes that maintain metal homeostasis (Fig. 1C),^{2,7,8} and metallochaperones deliver metals to proteins that need metal ions for function (Fig. 1D).^{9–12}

Both metal-sensing transcriptional regulation and metal trafficking involve dynamic cooperation of biomacromolecules. Diverse biochemical and biophysical characterizations have

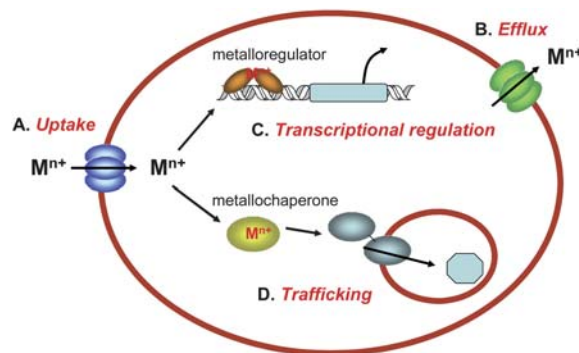


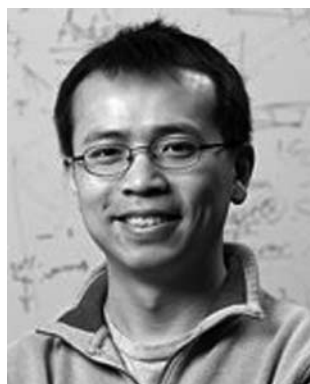
Fig. 1 Cellular processes for metal homeostasis. (A) Metal uptake. (B) Metal efflux. (C) Metal-sensing transcriptional regulation. (D) Metal trafficking.

Department of Chemistry and Chemical Biology, Cornell University, Ithaca, NY, 14853, USA. E-mail: pc252@cornell.edu

† This paper is part of an NPR themed issue on Metals in cells, guest-edited by Emma Raven and Nigel Robinson.

resulted in much knowledge about the individual players. These studies have revealed their functions, determined their structures, and identified their interaction partners. Still, much remains to be elucidated on how these biomacromolecules *work together* to

achieve their functions. For example, how do metalloregulators and DNA interact to control transcription? And, how do metallochaperones and their target proteins collaborate to deliver metal ions?



Peng Chen

Peng Chen received his B.S. from Nanjing University, China in 1997. After a year at University of California, San Diego, with Prof. Yitzhak Tor, he moved to Stanford University and did his Ph.D. with Prof. Edward Solomon in bio-inorganic/physical inorganic chemistry. In 2004, he joined Prof. Sunney Xie's group at Harvard University for post-doctoral research in single-molecule biophysics. He started his assistant professorship at

Cornell University in 2005. His current research focuses on single-molecule imaging of nanocatalysis and bioinorganic chemistry. He has received a Dreyfus New Faculty award, a NSF Career award, a Sloan Fellowship, and a Paul Saltman Award.



Aaron M. Keller

Aaron M. Keller grew up in Topeka, Kansas, where he received his B.S. in Chemistry at Washburn University. His undergraduate research experience involved modeling NMR spectra of cobalt bipyridal coordination compounds. He is currently a graduate student at Cornell University in the Department of Chemistry and Chemical Biology working for Prof. Peng Chen. Using single-molecule FRET in combination with nanovesicle trapping, he is

researching protein interactions between the copper chaperone, Hah1, and the Wilson's Disease Protein.



Nesha May Andoy

Nesha May Andoy obtained her B.S. in Chemistry at the University of the Philippines in 2001. She is currently a graduate student at Cornell University in the Department of Chemistry and Chemical Biology working in Prof. Peng Chen's group. Her research covers single-molecule studies of metalloregulator–DNA interactions, bioinorganic enzymology, and nanoscale catalysis.



Debashis Panda

Debashis Panda obtained his B.Sc. in chemistry from Calcutta University, India, in 2002, and received his M.Sc. (2004) and Ph.D. (2007) from the Indian Institute of Technology, Bombay. He is currently conducting his postdoctoral work on single-molecule protein–DNA interactions in Prof. Peng Chen's lab in the Department of Chemistry and Chemical Biology at Cornell University.



Jaime J. Benitez

Jaime J. Benítez was born and raised in San Juan, Puerto Rico. He obtained his B.S. in Chemistry from the University of Puerto Rico, Rio Piedras campus, in 2004. He is currently a Ph.D. graduate student, under Prof. Peng Chen, at Cornell University in the Department of Chemistry and Chemical Biology. His thesis work focuses on the characterization of protein–protein interaction dynamics from a single-molecule perspective.



Feng Gao

Feng Gao received his B.S. in chemistry from Nankai University in 1998 and his M.S. in chemistry from Peking University in 2001. He received his Ph.D. in chemistry from the University of Pennsylvania in 2007 under the supervision of Prof. Robin M. Hochstrasser. He is currently a postdoctoral fellow in Prof. Peng Chen's lab at Cornell University and studies protein–protein interactions involved in metal trafficking.

To address the above questions requires characterizing their underlying protein–DNA and protein–protein interactions. For studying these biological interactions, the single-molecule approach provides unique advantages: First, it removes ensemble averaging, so subpopulations, such as interaction intermediates, can be monitored and analyzed. Second, it removes the need for synchronization of molecular actions in studying time-dependent processes, as it monitors one molecule at a time. Third, it allows visualizing the actions of individual molecules in real time, and at any time point, only one molecular state is observed for one molecule even if the molecule can adopt multiple different states. This feature is particularly useful in capturing transient intermediates and elucidating the mechanism of molecular functions.

Single-molecule fluorescence techniques, such as single-molecule fluorescence resonance energy transfer (smFRET), are perhaps among the most popular because of their straightforward instrumentation and easy operation.^{13–16} Using confocal or total internal reflection (TIR) fluorescence microscopy to confine laser excitation to a small volume, and using low concentration (<10^{−9} M) to spatially separate fluorescent molecules, one can achieve fluorescence detection at the single-molecule level readily. Surface immobilization of molecules further allows following molecular actions over time. To apply smFRET, one attaches a FRET donor–acceptor pair to the target biomolecules and excites the fluorescence of the donor while monitoring the fluorescence intensities of both the donor (I_D) and the acceptor (I_A) simultaneously. The donor-to-acceptor FRET efficiency can be determined ($E_{\text{FRET}} \approx I_A/(I_A + I_D)$), which is directly correlated with the donor–acceptor interdistance, r , as $E_{\text{FRET}} = 1/[1 + (r/r_0)^6]$ (r_0 is the Förster radius of the specific FRET donor–acceptor pair). In this way, biological processes that involve distance changes, including protein–DNA and protein–protein interactions, can be studied by smFRET measurements.^{14–16}

Our group has been developing smFRET-based methods to tackle questions related to metal-sensing transcriptional regulation and metal trafficking, as part of our efforts in integrating single-molecule research to the field of bioinorganic chemistry.¹⁷ We have focused on two specific systems: (1) the bacterial MerR-family metalloregulators involved in metal-sensing transcriptional regulation,^{18,19} and (2) the human copper chaperones and their target transport proteins involved in intracellular copper trafficking.^{20–22} Here we review our recent progress in these two areas. For each area, we introduce the biological problem, identify the technical challenge, outline our methodology, and present case studies for gaining functional insights. At the end, we discuss remaining challenges.

2 Metal-sensing transcriptional regulation

2.1 MerR-family metalloregulators: protein–DNA interactions of subtle structural changes as a challenge

Metal-sensing transcriptional regulation is a key component of metal homeostasis.^{2,3,7,23–29} Bacteria, being susceptible to either limiting or toxic levels of metal ions in their living environment, have evolved highly sensitive and selective metal-sensing metalloregulators.^{3,6,23–33}

A large class of bacterial metalloregulators belong to the MerR-family; they respond to metal ions such as Hg²⁺, Pb²⁺ and Cu¹⁺ with high selectivity and sensitivity.^{8,23,24,33–36} All MerR-family regulators are homodimers with two DNA-binding domains. They regulate gene transcription *via* a DNA distortion mechanism,^{24,34,35,37,38} in which both the apo- and the holo-regulator bind tightly to a dyad-symmetric DNA sequence in the promoter region, with one DNA-binding domain binding to each half of the dyad sequence. In the apo-regulator bound form, DNA is slightly bent (~50°) and the transcription is suppressed. Upon metal binding, the holo-regulator further unwinds DNA slightly (~30°), and transcription is activated. As the regulator–DNA interactions dictate the transcription process, defining the associated protein–DNA interactions quantitatively is crucial for understanding their structure–dynamics–function relationships.

SmFRET measurements are powerful in studying protein–DNA interactions and associated structural changes of proteins and DNA.^{14–16} Experimentally, smFRET techniques rely largely on detecting nanometer-scale structural changes. This is inherently related to both the FRET mechanism and the fluorescent probes suitable for single-molecule detection.^{15,39} Many DNA-binding proteins, including MerR-family metalloregulators,^{24,34,35,37,38} merely cause DNA structural changes of Angstrom scale, however. A method that enables smFRET study of protein–DNA interactions while alleviating this hindrance is therefore desirable. To this end, we have developed engineered DNA Holliday junctions (HJs) as single-molecule reporters in smFRET measurements for studying protein–DNA interaction.^{18,19}

2.2 Methodology: engineered DNA Holliday junctions as smFRET reporters for protein–DNA interactions

Our method builds on the intrinsic structural dynamics of DNA HJs and the ease of following their dynamics by smFRET. HJs are four-way DNA junctions that form during homologous DNA recombination.^{40–42} In the presence of Na⁺ and Mg²⁺, each HJ molecule folds into two X-shaped stacked conformers by pairwise stacking of its four helical arms (conf-I and conf-II, Fig. 2A). In one conformer, two of the DNA strands run through a pair of stacked helical arms similarly as in a B-form DNA, while the other two strands exchange between stacked helical pairs (Fig. 2B).^{43,44} The four strands switch positions in the other conformer. These two stacked conformers exist in a dynamic equilibrium at room temperature (Fig. 1A). With a FRET donor–acceptor pair labeled at the ends of two HJ arms, the two conformers have distinct FRET signals, one having higher FRET efficiency (E_{FRET}) and the other lower E_{FRET} . The interconversion dynamics between the two conformers are reflected by the two-state fluctuation behavior in the E_{FRET} trajectories of single molecules.^{18,19,41,45}

To use a HJ as a smFRET reporter for protein–DNA interactions, we encode in its arms the dyad-symmetric sequence recognized by a metalloregulator (Fig. 2A). Because the part of DNA that contains the encoded sequence has distinct spatial orientations in the two conformers, the metalloregulator binds to the two conformers differentially and causes changes in their structures and their interconversion dynamics. These changes are readily measurable by smFRET and thus report the associated

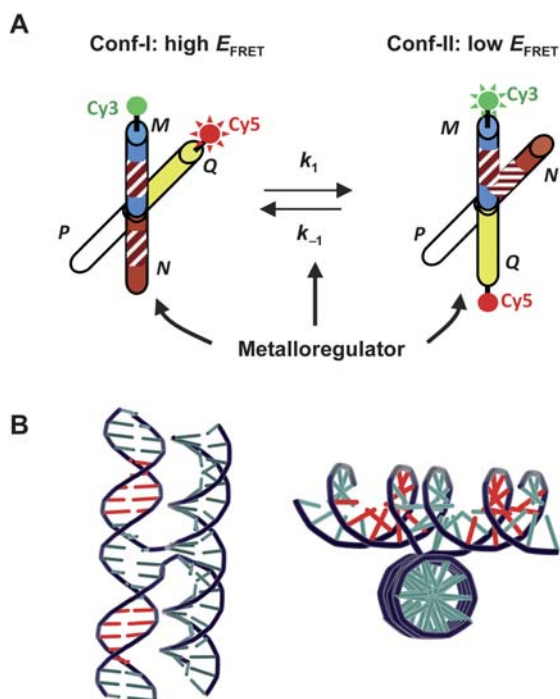


Fig. 2 Engineered DNA Holliday junctions (HJs) as smFRET reporters for protein–DNA interactions. (A) Structural dynamics of an engineered HJ between its two conformers, conf-I and conf-II. Cy3 and Cy5 are labeled at the ends of arms *M* and *Q* to differentiate conf-I (high E_{FRET}) and conf-II (low E_{FRET}). The stripes on arms *M* and *N* indicate the encoded dyad-symmetric sequence recognized by a metalloregulator. Protein binding will perturb both the structures and the dynamic equilibrium of the HJ, which are readily followed by the FRET signal. (B) Structural model of a stacked HJ conformer in two different orientations. The dyad-symmetric sequence is highlighted in red as in conf-I. Figures adapted from ref. 18 and 19.

protein–DNA interactions. This is a generalizable approach, since we can encode into HJs various sequences recognizable by many DNA-binding proteins. As the effects of protein actions on DNA are converted to and amplified by the changes in the structures and dynamics of the engineered HJ, it is possible to study protein–DNA interactions that involve merely small structural changes.^{18,19}

2.3 Application to interactions of PbrR691 and CueR with DNA

We have applied the above methodology to study the interactions with DNA of two MerR-family metalloregulators: PbrR691, a Pb^{2+} -responsive regulator from *Ralstonia metallidurans*,¹⁸ and CueR, a Cu^{1+} -responsive regulator from *Escherichia coli*.¹⁹ For each of them, we designed an engineered HJ, in which the protein-recognition dyad-symmetric sequence spans the arms *M* and *N* as depicted in Fig. 2A. These sequences ensure specific recognitions by the proteins of interest. The FRET pair Cy3 and Cy5 are attached at the ends of arms *M* and *Q* for smFRET measurements. A biotin label at the end of arm *P* is used for surface-immobilization *via* a biotin–streptavidin linkage, so the fluorescence signals of individual HJ molecules can be followed over time.

The intrinsic structural dynamics of the engineered HJs is clear in the E_{FRET} *versus* time trajectory of a single HJ molecule – its E_{FRET} shows reversible transitions between a high and a low E_{FRET} state, corresponding to the structural interconversions between conf-I and conf-II (Fig. 3A). In this E_{FRET} trajectory, the two so-called “waiting times”, τ_{I} and τ_{II} , are important observables. τ_{I} is the waiting time for conf-I to conf-II transition, while τ_{II} is the waiting time for conf-II to conf-I transition. Their individual values are stochastic; some of them longer, some shorter; but their statistical properties, such as their distributions and averages, are defined by the underlying kinetics of the HJ structural dynamics. For a two-state interconversion scheme as in Fig. 2A, the inverse of average waiting times follow:

$$\langle \tau_{\text{I}} \rangle^{-1} = 1 / \int_0^{\infty} \tau f_{\text{I}}(\tau) \, d\tau = k_{-1} \quad \text{and} \quad \langle \tau_{\text{II}} \rangle^{-1} = 1 / \int_0^{\infty} \tau f_{\text{II}}(\tau) \, d\tau = k_1$$

Here $\langle \dots \rangle$ denotes averaging; $f_{\text{I}}(\tau)$ and $f_{\text{II}}(\tau)$ are the probability density functions of τ_{I} and τ_{II} ; k_1 and k_{-1} are the interconversion rate constants. Sometimes τ_{I} and τ_{II} are also termed “dwell times”. Their averages, $\langle \tau_{\text{I}} \rangle$ and $\langle \tau_{\text{II}} \rangle$, represent the lifetimes of conf-I and conf-II, and are equal to $1/k_{-1}$ and $1/k_1$, respectively.

Upon introducing a metalloregulator, protein binding causes significant changes in the structural dynamics of the engineered

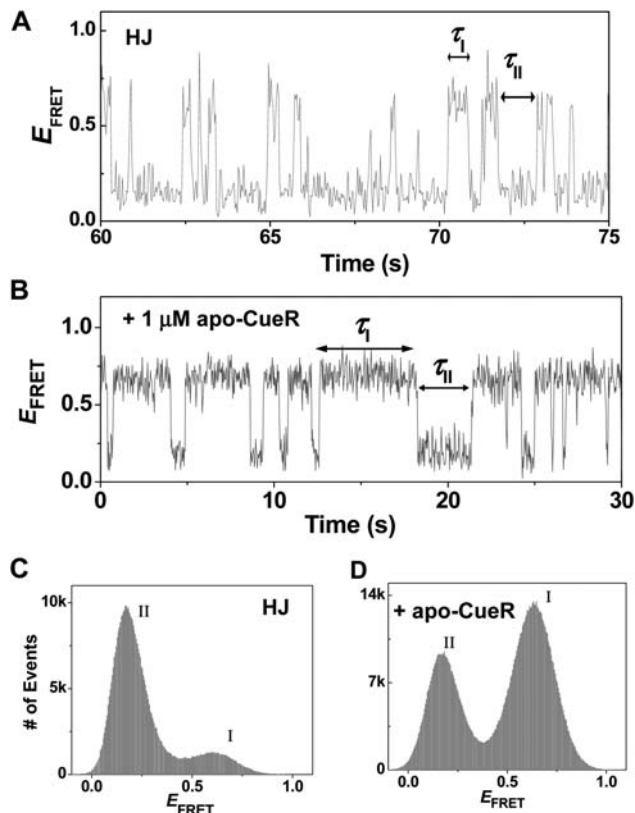


Fig. 3 CueR-imposed HJ structural equilibrium shift. (A, B) Exemplary single-molecule E_{FRET} trajectories of a CueR-specific HJ in the absence (A) and presence (B) of 1.0 μM apo-CueR. E_{FRET} is approximated as $I_{\text{Cy5}}/(I_{\text{Cy3}} + I_{\text{Cy5}})$ (*I*: fluorescence intensity). τ_{I} and τ_{II} are the waiting times on the E_{FRET} states of conf-I and conf-II, respectively. (C, D) Histograms of E_{FRET} trajectories in the absence (C) and presence (D) of 1.0 μM apo-CueR. Figures adapted from ref. 19.

HJ. Below we summarize what the actions of the metallorepressor PbrR691 and CueR are on the engineered HJ (*i.e.*, DNA) and how to determine them by analyzing the time-dependent E_{FRET} of single molecules, *i.e.*, the single-molecule E_{FRET} trajectories.

Preferential protein binding to and stabilization of conf-I. Due to the different spatial arrangements of arms M and N , which contain the dyad-symmetric sequence, both PbrR691 and CueR preferentially bind and stabilize conf-I relative to conf-II, regardless of the proteins' metallation state. This preferential stabilization of conf-I is manifested by an equilibrium shift of the HJ structural dynamics toward conf-I: the E_{FRET} trajectory of a single HJ molecule shows that the molecule spends more time on the high E_{FRET} state, *i.e.*, conf-I (Fig. 3B). This equilibrium shift is clearer in the histograms of the E_{FRET} trajectories, which have two peaks, one at a higher E_{FRET} and the other at a lower E_{FRET} , corresponding to conf-I and conf-II, respectively (Fig. 3C). In the presence of the apo- or the holo-metallorepressors, the intensity of the peak corresponding to conf-I increases relative to that of conf-II (Fig. 3D). This preferential stabilization of conf-I reflects the metalloregulators' normal function as double-strand DNA-binding proteins, because conf-I has arms M and N coaxially stacked as in a B-form DNA (Fig. 2).

Kinetic scheme of protein interactions with the engineered HJ.

In the single-molecule E_{FRET} trajectories, the two waiting times, τ_I and τ_{II} , contain the kinetic information about the structural interconversions between the two HJ conformers. Upon interaction with a metalloregulator, the changes of the interconversion kinetics report the kinetic scheme of the protein–HJ interactions. In our study of CueR–HJ interactions, we found that the apo-CueR interactions with the two HJ conformers follow different kinetic mechanisms. It binds to conf-I to form a complex (P-I) that does not lead to structural transition to conf-II (Fig. 4A, red box). On the other hand, it interacts with conf-II in a two-step manner – it initially binds to conf-II to form a complex (P-II) that can lead to structural transition to conf-I; this P-II complex can then bind a second protein molecule to form a tertiary complex (P₂-II) that does not lead to structural transition to conf-I (Fig. 4A, green box).

Experimentally, the interaction kinetic scheme of apo-CueR with conf-I is manifested by the protein concentration ([P]) dependence of $\langle\tau_I\rangle^{-1}$, the time-averaged single-molecule rate of conf-I \rightarrow conf-II transition. With increasing [P], $\langle\tau_I\rangle^{-1}$ decreases asymptotically to zero (Fig. 4B, solid circles), because the formed P-I complex cannot lead to structural transition. This [P] dependence is described quantitatively by the following equation:

$$\langle\tau_I\rangle^{-1} = \frac{k_1}{1 + [P]/K_{P-I}} \quad (1)$$

where $K_{P-I} (= k_{-2}/k_2)$ is the dissociation constant for the apo-CueR–conf-I complex, and k_2 and k_{-2} are the protein binding and unbinding rate constants to conf-I, respectively.

The two-step kinetic scheme of the apo-CueR interaction with conf-II is manifested by the biphasic [P] dependence of $\langle\tau_{II}\rangle^{-1}$, the time-averaged single-molecule rate of conf-II \rightarrow conf-I transition. With increasing [P], $\langle\tau_{II}\rangle^{-1}$ initially increases, reflecting the formation of complex P-II that helps structural transition to

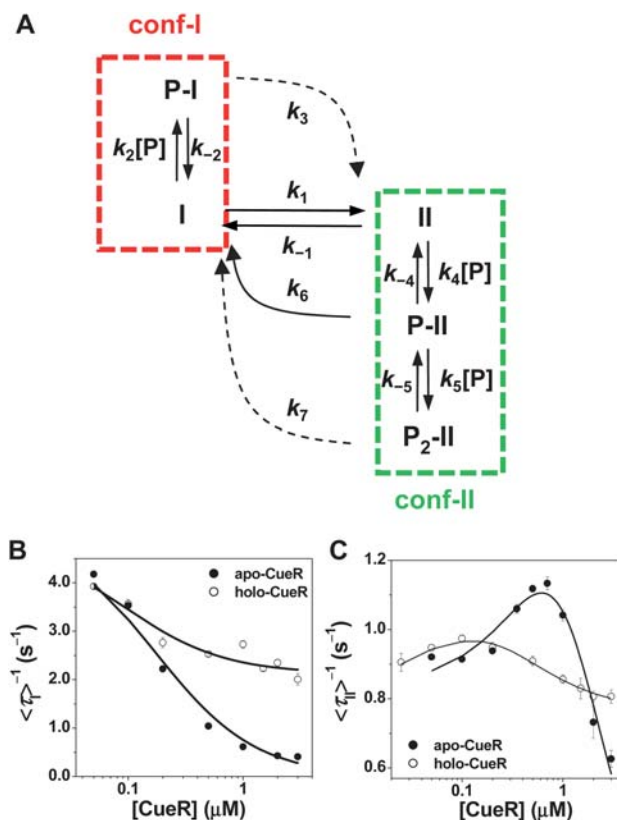


Fig. 4 CueR–HJ interaction kinetics. (A) Interaction kinetic scheme between the engineered HJ and CueR. I, conf-I; II, conf-II; P, apo-CueR or holo-CueR; and rate constants, k . The k_3 and k_7 processes are only for holo-CueR. (B, C) Apo-CueR (●) and holo-CueR (○) concentration dependence of $\langle\tau_I\rangle^{-1}$ (B) and $\langle\tau_{II}\rangle^{-1}$ (C). The solid lines are the fits with equations describing the [P] dependence of $\langle\tau_I\rangle^{-1}$ and $\langle\tau_{II}\rangle^{-1}$. Figures adapted from ref. 19.

conf-I (Fig. 4C, solid circles); and it decays at higher [P] after reaching a maximum, reflecting the subsequent formation of the tertiary complex P₂-II that cannot lead to structural transition. This [P] dependence is quantitatively described by the following equation:

$$\langle\tau_{II}\rangle^{-1} = \frac{k_{-1} + \frac{k_6[P]}{K'_{P-II}}}{1 + \frac{[P]}{K'_{P-II}} + \frac{[P]^2}{K'_{P-II}K_{P_2-II}}} \quad (2)$$

where $K'_{P-II} (= (k_{-4} + k_6)/k_4)$, $K_{P_2-II} = k_{-5}/k_5$, and k values are the rate constants defined in Fig. 4A.

Holo-CueR interactions with the HJ show many similarities to those of apo-CueR, but significant differences also exist. Unlike apo-CueR, the P-I complex and the tertiary P₂-II complex involving holo-CueR can still allow structural transitions from one HJ conformer to the other (k_3 and k_7 in Fig. 4A). These additional kinetic processes in holo-CueR–HJ interactions are manifested by the holo-CueR concentration dependence of $\langle\tau_I\rangle^{-1}$ and $\langle\tau_{II}\rangle^{-1}$ – at high [P], neither $\langle\tau_I\rangle^{-1}$ nor $\langle\tau_{II}\rangle^{-1}$ decays to zero, and instead they approach a constant value. Incorporating these two additional kinetic processes, equations similar to eqn (1) and (2) can be derived to describe the [P] dependence of $\langle\tau_I\rangle^{-1}$ and $\langle\tau_{II}\rangle^{-1}$ quantitatively (Fig. 4B, C).

The differences between apo- and holo-CueR interactions with the HJ have functional implications. Conf-I and conf-II are significantly different in their spatial arrangements of the dyad-symmetric sequence (Fig. 2B). Being more accommodating in allowing HJ structural interconversion suggests that holo-CueR has more flexible conformation than apo-CueR. This additional conformational flexibility of holo-CueR could play important roles in its interaction with the RNA polymerase (RNAP) for transcription, as past studies on MerR, the prototype MerR-family metalloregulator, showed that the holo-MerR-DNA-RNAP tertiary complex undergoes structural rearrangements in transcriptional initiation.^{24,34,35,46}

There is also a difference between CueR and PbrR691. Although both apo- and holo-CueR can form the tertiary complex P₂-II with conf-II, this tertiary complex is not observed in PbrR691-HJ interactions, suggesting that differences exist among MerR-family metalloregulators in their interactions with DNA.

Protein-induced DNA structural changes. The metalloregulator binding also causes structural changes of the HJ, *i.e.*, the DNA. The structural change of conf-I in the P-I complex is particularly of interest, because conf-I mimics the metalloregulators' natural substrate, with its arms *M* and *N* stacked into a helix (Fig. 2A and B). For both CueR and PbrR691, regardless of their metallation state, we found that the protein-caused structural changes of conf-I are consistent with the bending of its *M*-*N* helix (Fig. 5A). This *M*-*N* helix bending leads to a shortened distance between the ends of the arms *M* and *Q* where the two FRET probes are located (Fig. 5A). This shortened distance between the FRET probes results in an increase in the E_{FRET} value of conf-I ($E_{\text{conf-I}}$) upon metalloregulator binding, detectable by our smFRET measurements (Fig. 5B, C, and D).

Fig. 5E gives a structural model of how a MerR-family metalloregulator may bind to conf-I. Since no structural information is yet available for PbrR691 and CueR in complex with DNA, we used the structural data of the MtaN-DNA complex³⁸ to construct the model by adjusting and aligning the stacked *M*-*N* helix with the DNA structure in the MtaN-DNA complex. (MtaN is also MerR-family regulator; it responds to organic molecules instead of metal ions.) The structural model shows that the protein binds to the major grooves at the dyad-symmetric sequence and the *M*-*N* helix bending leads to a closer distance between the ends of arms *M* and *Q*.

It is worth noting that it is nontrivial to detect the helix bending by MerR-family metalloregulators. Assuming a $\sim 130^\circ$ bending angle from the crystal structure of the MtaN-DNA complex,³⁸ the estimated end-to-end distance change is only ~ 0.8 nm for a 24 base-pair DNA helix having a contour length of ~ 8.2 nm. The small distance change is challenging to detect with smFRET measurements, and indeed we did not observe discernable change in E_{FRET} when we put the two FRET probes at the ends of arms *M* and *N*.¹⁸ Making a longer DNA helix will generate a large end-to-end distance change upon bending, but the distance to be measured will be out of the nanometer distance range that smFRET is sensitive to. So instead of trying to detect directly the end-to-end distance changes of the conf-I *M*-*N* helix, our approach using engineered HJs circumvents this problem by measuring the distance changes between the ends of arms *M* and *Q*. (Fig. 5A). The relative position of arms *M* and *Q* are coupled

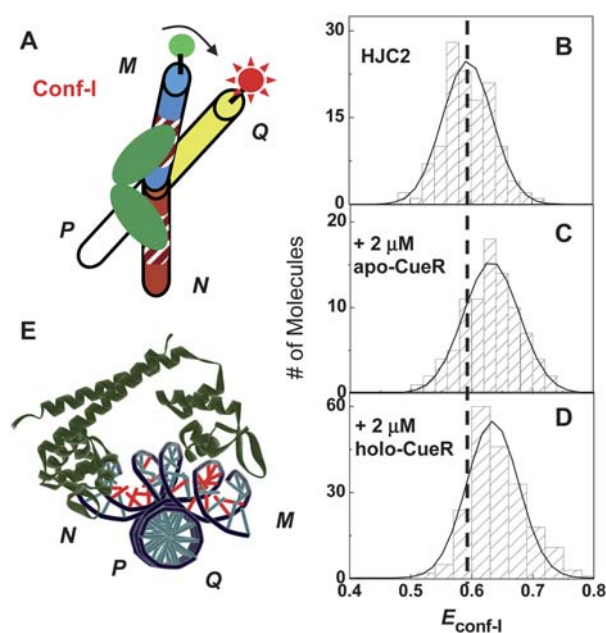


Fig. 5 Metalloregulator-imposed HJ structural change. (A) Scheme of metalloregulator interaction with HJ conf-I, showing protein-imposed *M*-*N* helix bending that leads to a shortened distance between the FRET donor and the acceptor. (B, C, D) Histograms of $E_{\text{conf-I}}$ of the CueR-specific HJ in the absence and presence of apo-CueR and holo-CueR. The histograms show that $E_{\text{conf-I}}$ increases upon metalloregulator binding. (E) Structural model of MtaN (PDB code 1R8D)³⁸ bound to HJ conf-I, showing the bending distortion of the *M*-*N* helix. Figures adapted from refs. 18 and 19.

to *M*-*N* helix bending because of the junction connection, thus enabling studies of small bending motions of the DNA helix imposed by MerR-family metalloregulators.

Implications for transcriptional suppression after activation.

From the single-molecule kinetics of protein-HJ interactions, the binding affinities of the proteins to the two HJ conformers can also be obtained. For both CueR and PbrR691, their holo forms bind stronger to the HJ than the apo forms do, irrespective of the HJ conformation. For CueR, for example, this stronger DNA binding affinity is reflected by the slightly faster decay of $\langle \tau_1 \rangle^{-1}$ and by the clear earlier maximum of $\langle \tau_{11} \rangle^{-1}$ with increasing [holo-CueR] (Fig. 4B, C). For both CueR and PbrR691, the holo form's stronger DNA binding affinities are further confirmed in their interactions with simple double-strand DNA.¹⁹

The stronger DNA binding affinity of the holo form is surprising, however, as past studies on MerR have shown that holo-MerR binds more weakly to DNA than apo-MerR does.³⁴ As the direct dissociation of the metal ion from the metalloregulators is believed to be difficult due to strong metal coordination, it was thought that the weaker binding of holo-protein would facilitate its replacement from the DNA by the apo-protein, thus switching off the transcription after transcriptional activation and once the cell is relieved of the metal stress.²⁴ Therefore, the opposite relative DNA binding affinities of apo *versus* holo protein for CueR/PbrR691 suggests possible differences in the mechanism by which MerR-family metalloregulators switch off transcription.

Moreover, unlike MerR, which might involve another protein MerD to help the dissociation of the holo-MerR–DNA complex,³³ no evidence has yet been found for a co-regulator role of a MerD homologue in the regulatory mechanism of CueR or PbrR691.³³ For CueR/PbrR691 to switch off transcription after activation, one simple scenario is a direct dissociation of the holo-protein from DNA followed by binding of the apo-protein, which would be the dominant form of the metalloregulator inside the cell after activation of metal-resistance genes. For this scenario to be viable, the dissociation kinetics of the holo-protein from DNA has to be in a relevant timescale to gene regulation. From our single-molecule kinetic analyses of metalloregulator–HJ interactions, the rate constants for protein unbinding and binding to the HJ conf-I cannot be obtained. Nevertheless, as the protein binding and unbinding are contained in the observed structural dynamics of the HJ, which we measure experimentally, protein binding and unbinding should occur at a comparable timescale to HJ's structural dynamics, *i.e.*, hundreds of milliseconds to seconds, a relevant timescale for gene expression regulation.

3 Intracellular copper transport

3.1 Copper chaperones: weak, dynamic protein interactions as a challenge

Metal trafficking is another important process that is regulated for metal homeostasis.^{2,4,9–12} Through specific metal transporters, such as metallochaperones, metal ions are delivered to their target locations while avoiding fortuitous binding by many other cellular molecules. Inside cells, copper chaperones mediate the trafficking of copper ions.^{9,10,47,48} In human cells, the copper chaperone Hah1 (also named Atox1) delivers Cu¹⁺ ions to two homologous copper-transporting ATPases: Wilson disease protein (WDP) and Menkes disease protein (MNK).^{49–52}

We are particularly interested in the Hah1–WDP copper transport pathway. Hah1 is a single-domain, cytoplasmic protein belonging to the Atx1-family.¹⁰ WDP is a multi-domain protein anchored on organelle membranes and has a cytosolic N-terminal region consisting of six metal-binding domains (MBDs).^{53,54} The six WDP MBDs and Hah1 are homologous with the same $\beta\alpha\beta\beta\alpha\beta$ protein fold, and all of them contain a conserved, surface-exposed CXXC motif that binds Cu¹⁺ with the two cysteines. The similar protein fold of Hah1 and WDP MBDs and their complementary surface residues render their specific interactions; Cu¹⁺ can be transferred from the copper binding site of Hah1 to that of a WDP MBD through *direct* Hah1–MBD interaction and a ligand exchange mechanism.^{9,47,51,55–57}

Past studies have shown that the six MBDs of WDP have different functional roles.^{51,58–64} MBDs 1 to 4 are important for interaction with Hah1 to acquire Cu¹⁺, and MBDs 5 and 6 are critical for copper translocation through organelle membranes. Yet, all six WDP MBDs, as well as Hah1, have similar Cu¹⁺ binding affinities.^{63,65} This similarity in Cu¹⁺ binding affinity indicates that Cu¹⁺ transfer from Hah1 to WDP is under kinetic control mediated by Hah1–WDP interactions and that the functional differences among WDP MBDs are not defined by their Cu¹⁺ binding affinity but may be related to *how* each MBD

interacts with Hah1. Quantifying how Hah1 and WDP interact is thus crucial for understanding this protein-interaction-mediated copper transfer process.

Yet, few quantitative studies are available on protein interaction dynamics of copper chaperones. Surface plasmon resonance (SPR) has been used to study the association and dissociation kinetics of Hah1–MNK and related bacterial chaperones.^{66,67} These SPR studies employ proteins that are immobilized on surfaces nonspecifically and in random orientations. NMR has also been used to study the copper chaperone–target protein interactions,^{53,58,59,68–70} but only estimates have been obtained on the timescales of their interaction dynamics.

The scarcity of quantitative information on the involved protein interaction dynamics is not surprising, for these interactions are weak, which makes them difficult to quantify in conventional measurements where the behavior of an ensemble of molecules are examined. Many aspects contribute to this difficulty: (1) Weak protein interactions are dynamic and stochastic, making synchronization of molecular actions often necessary. (2) The steady-state concentrations of interaction intermediates are often low, making detection difficult. (3) Multiple interaction intermediates, if present, convolute the ensemble-averaged measurements.

Single-molecule measurements offer several advantages for studying weak protein interaction. (1) No synchronization of molecular actions is necessary. (2) Molecular actions are followed in real time, including the formation, interconversion, and dissolution of interaction intermediates. (3) Only one molecular state, be it an intermediate, is observed at any time point, enabling the resolution of complex interaction kinetics. Among the many single-molecule measurements, smFRET, with its inherent distance dependence, is particularly suited for studying dynamic protein interactions, which is accompanied by changes in inter-protein distances.

Still, there are technical challenges to overcome before smFRET measurements can be applied to follow weak protein interactions in real time. The primary challenge is the typical pM–nM fluorophore concentration employed in single-molecule fluorescence measurements to separate fluorophores spatially. This low concentration limits single-molecule protein interaction studies to strong interacting pairs. Weak protein interactions, such as Hah1–WDP interactions, need to be studied at much higher concentrations (>10^{−6} M) to favor complex formation. Nonspecific protein–glass surface interactions during surface immobilization present another challenge; they must be minimized. To overcome these challenges, we have adapted a nanovesicle trapping strategy to enable smFRET study of Hah1–WDP interactions.^{20–22} This nanovesicle trapping strategy has also been used in single-molecule studies of enzyme reactions,⁷¹ protein folding,^{72–75} nucleic acid conformational dynamics,^{76,77} and protein–nucleic acid interactions.^{78,79}

3.2 Methodology: nanovesicle trapping combined with smFRET

Fig. 6 depicts our nanovesicle trapping strategy. We trap two interacting molecules inside a 100 nm lipid vesicle. Because of the confined volume (~10^{−19} L), the effective concentration is a few micromolar for each molecule inside. We then keep the overall

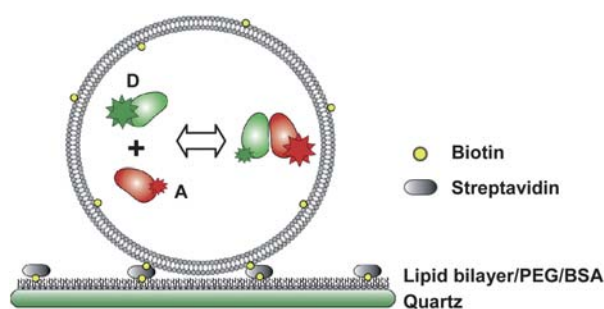


Fig. 6 Schematic of nanovesicle trapping of two proteins labeled with a FRET donor–acceptor pair for smFRET studies. The glass surface is coated with PEG, lipid bilayer or biotinylated BSA to prevent vesicle rupture.

number of nanovesicles low to separate individual nanovesicles spatially to achieve single-vesicle (*i.e.*, single-pair) detection condition. The nanovesicles are then immobilized on the surface, where the nonspecific protein interactions with the glass surface are eliminated. Although we cannot ensure that every nanovesicle will contain two different molecules, the statistical distribution of molecules in nanovesicles can be controlled, and for each nanovesicle, the number and type of molecules in it are easily identified by monitoring the discrete photobleaching events of the donor and acceptor probes under single-molecule imaging conditions.²² Nanovesicle trapping also eliminates the complication of dimeric or multimeric interactions among molecules of the same type. If self-dimerization or oligomerization exists, it is unavoidable in ensemble experiments and can significantly complicate protein interaction studies. This complication is particularly relevant in studies of Hah1–WDP interactions, as Hah1 (and likely WDP MBDs) can form dimers in solution.^{10,56}

With the two interacting molecules labeled with a FRET donor–acceptor pair (*e.g.*, Cy3 and Cy5), we can visualize their interactions in real time using smFRET measurements at high effective concentrations. This nanovesicle trapping approach is general and can be applied to study many other weak protein interactions.

3.3 Application to interactions between the copper chaperone Hah1 and the Wilson disease protein

We have applied the above methodology to study the interactions between Hah1 and the fourth MBD (MBD4) of WDP in the absence of Cu^{1+} .^{20–22} We chose MBD4 as a representative WDP MBD because it is known to interact with Hah1 directly for Cu^{1+} transfer.^{51,59,64} Quantification of Hah1–MBD4 interaction dynamics will provide foundation for understanding how Hah1 and the full length WDP interact for Cu^{1+} transfer. We labeled Hah1 with the FRET acceptor Cy5 and MBD4 with the donor Cy3 at a C-terminal cysteine site-specifically. Below we summarize the results from our smFRET measurements of the Hah1–MBD4 interaction dynamics and their functional implications.

Visualization of dynamic interactions and identification of multiple interaction complexes. Real-time smFRET

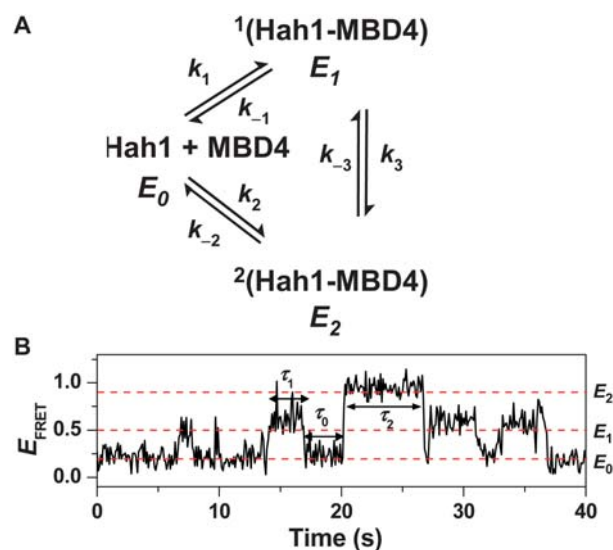


Fig. 7 Hah1–MBD4 interactions. (A) Interaction scheme between Hah1 and MBD4. (B) Exemplary E_{FRET} trajectory of a Cy5–Hah1 and a Cy3–MBD4 trapped in a 100-nm nanovesicle. Figures adapted from refs. 20 and 21.

measurements enables direct visualization of the dynamic interactions between Hah1 and MBD4, in which the interaction complexes form and dissolve continually (Fig. 7A). These dynamic interactions are reported by the temporal fluctuations of the E_{FRET} trajectories of each interacting pair between three distinct E_{FRET} states (Fig. 7B). A lower E_{FRET} reflects a longer distance between the molecules and a higher E_{FRET} reflects a shorter distance.

Besides the dissociated state, which has the lowest E_{FRET} of ~ 0.2 (denoted as E_0), the E_{FRET} trajectories reveal two different Hah1–MBD4 interaction complexes (Fig. 7B). These two complexes appear as the two higher E_{FRET} states at $E_{\text{FRET}} \approx 0.5$ and 0.9 (denoted as E_1 and E_2), and their higher E_{FRET} values result from the nanometer proximity of the two FRET labels in the complexes. The significant difference between E_1 and E_2 also indicates that the Cy3–Cy5 distances differ by nanometers between the two complexes. This nanometer distance difference likely arises from the differences in overall interaction geometries of these two complexes, rather than in the conformation of one or both proteins, because past NMR studies showed that Hah1 and MBD4 only have Angstrom-scale conformational flexibilities.^{53,70,80} The direct resolution of two distinct interaction complexes is exciting, as it is the first evidence that multiple interaction intermediates exist for metallochaperone–target protein interactions, and it definitely shows that Hah1 forms complexes with WDP despite the absence of Cu^{1+} .

Determination of interaction complex stability. The direct resolution of distinct interaction complexes also enables quantification of their stabilities for the first time. The histogram of the E_{FRET} trajectories shows three peaks, centered at E_0 , E_1 , and E_2 , corresponding to the dissociated state and the two interaction complexes, respectively (Fig. 8). The relative intensities of these three peaks directly reflect their relative stabilities. The

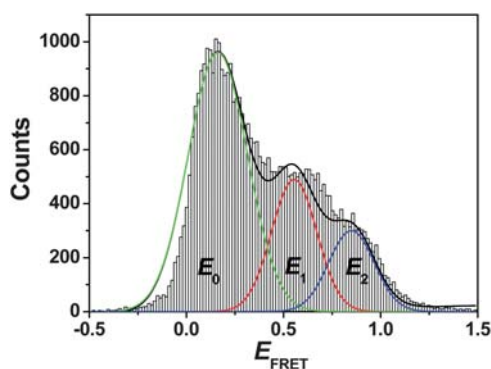


Fig. 8 Histogram of E_{FRET} trajectories of Hah1-MBD4 interacting pairs. The histogram shows three peaks corresponding to E_0 , E_1 , and E_2 states. Figure adapted from refs. 20 and 21.

determined dissociation constants of the two interaction complexes are $K_{\text{D1}} = 5 \pm 1 \mu\text{M}$ and $K_{\text{D2}} = 8 \pm 2 \mu\text{M}$.

Although complex 1 is clearly more stable, the dissociation constants of the two interaction complexes are within the same magnitude. For ensemble-averaged measurements, their similarity in stability is a challenge, as the two complexes always coexist. Without differentiated detection, the measured effective dissociation constant ($K_{\text{D,eff}}$), if obtainable, would be a geometric average of the K_{D} values of the two complexes, as $1/K_{\text{D,eff}} = 1/K_{\text{D1}} + 1/K_{\text{D2}}$.

Quantification of interaction kinetics. The real-time observation of the dynamic interactions of single Hah1-MBD4 pairs makes it possible to quantify their interaction kinetics. In the E_{FRET} trajectories, the transitions between E_0 and E_1 states and between E_0 and E_2 states correspond to the binding and unbinding processes of complex 1 and 2, and the transitions between E_1 and E_2 are the interconversions between the two complexes. The statistical properties of the waiting times (τ_0 , τ_1 , and τ_2 , Fig. 7B) on the three E_{FRET} states before each transition are defined by the interaction kinetics.

Using the interaction scheme in Fig. 7A, the probability density functions $f(\tau)$ of τ_0 , τ_1 , and τ_2 are related to the kinetic parameters as:

$$f_0(\tau) = (k_1 + k_2)c_{\text{eff}} \exp[-(k_1 + k_2)c_{\text{eff}}\tau] \quad (3a)$$

$$f_1(\tau) = (k_{-1} + k_3) \exp[-(k_{-1} + k_3)\tau] \quad (3b)$$

$$f_2(\tau) = (k_{-2} + k_{-3}) \exp[-(k_{-2} + k_{-3})\tau] \quad (3c)$$

where c_{eff} is the effective concentration of a single molecule inside a nanovesicle. Therefore, fitting the distributions of τ_0 , τ_1 , and τ_2 with exponential functions gives $k_1 + k_2$, $k_{-1} + k_3$, and $k_{-2} + k_{-3}$ directly (Fig. 9). Furthermore, the waiting time τ_0 can be separated into two subtypes: one $\tau_{0 \rightarrow 1}$ that precedes an $E_0 \rightarrow E_1$ transition and the other $\tau_{0 \rightarrow 2}$ that precedes an $E_0 \rightarrow E_2$ transition. Similarly, τ_1 can be separated into $\tau_{1 \rightarrow 0}$ and $\tau_{1 \rightarrow 2}$ subtypes, and τ_2 into $\tau_{2 \rightarrow 0}$ and $\tau_{2 \rightarrow 1}$ subtypes. The ratios between the occurrences (N) of the waiting time subtypes are also determined by the kinetic rate constants:

$$N_{0 \rightarrow 1}/N_{0 \rightarrow 2} = k_1/k_2 \quad (4a)$$

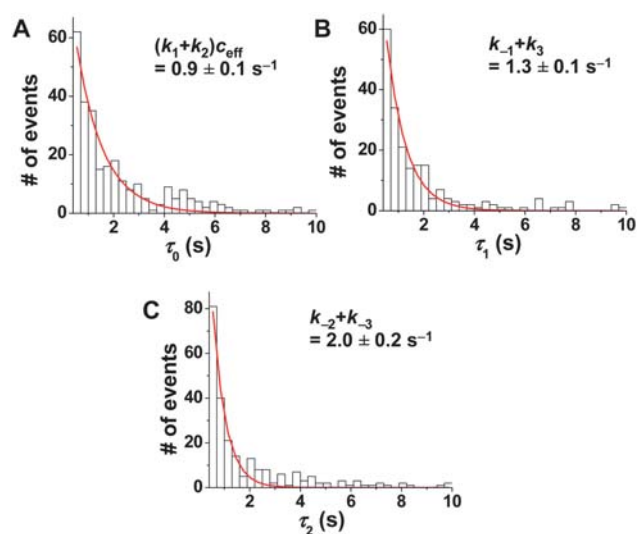


Fig. 9 Distributions of the waiting times τ_0 , τ_1 , and τ_2 from E_{FRET} trajectories of Hah1-MBD4 interactions. Solid lines are exponential fits; insets give the decay constants of the exponential fits and the relations to the protein-interaction rate constants. c_{eff} ($\sim 3 \mu\text{M}$) is the effective concentration of a single molecule in a 100 nm nanovesicle. The individual rate constants are: $k_1 \sim 1.6 \times 10^5 \text{ M}^{-1} \text{ s}^{-1}$, $k_{-1} \sim 0.9 \text{ s}^{-1}$, $k_2 \sim 1.4 \times 10^5 \text{ M}^{-1} \text{ s}^{-1}$, $k_{-2} \sim 1.3 \text{ s}^{-1}$, $k_3 \sim 0.4 \text{ s}^{-1}$, and $k_{-3} \sim 0.7 \text{ s}^{-1}$. Figures adapted from refs. 20 and 21.

$$N_{1 \rightarrow 0}/N_{1 \rightarrow 2} = k_{-1}/k_3 \quad (4b)$$

$$N_{2 \rightarrow 0}/N_{2 \rightarrow 1} = k_{-2}/k_{-3} \quad (4c)$$

Combining eqns (3a-c) and (4a-c), we can determine the individual rate constants for Hah1-MBD4 interactions (Fig. 9, caption). It is particularly exciting to be able to quantify both k_3 and k_{-3} , the rate constants of interconversion between the two transient interaction complexes. Ensemble measurements of interconversions dynamics normally can only obtain the sum of these two rate constants; here, by real-time visualization of the interconversion kinetics in both directions, we are able to determine each of the rate constants. From the rate constants, dissociation constants of both interaction complexes can also be obtained, with $K_{\text{D1}} = 6 \pm 1 \mu\text{M}$ and $K_{\text{D2}} = 9 \pm 1 \mu\text{M}$, consistent with those from analyzing the E_{FRET} histogram (Fig. 8).

Functional significance of dynamic protein interactions. The discovery of multiple interaction complexes and the quantification of interaction dynamics bring insights into the role of protein interactions for metal transfer. Inside cells, the copper chaperones encounter their target proteins through diffusion. The initial encounter pair often rapidly returns to the dissociated form.⁸¹ The ability to form multiple complexes with different geometries increases the probability of complex formation. The formed complex, if productive, may proceed to accomplish Cu^{1+} transfer, or if unproductive, convert to another complex for Cu^{1+} transfer. For this scenario to be viable, the complex interconversion kinetics should then be comparable to or faster than the dissociation kinetics. In the case of Hah1-MBD4 interactions, the rate constants of interconversions (k_3 and k_{-3}) are comparable to those of dissociations (k_{-1} and k_{-2}) (Fig. 9, caption).

Nonetheless, there is a balance for the multiplicity of complex formation to assist Cu^{1+} transfer function – if too many interaction complexes exist, sampling all complexes before reaching a productive complex could be time-costly.

Furthermore, WDP is not a single-domain protein, but rather has six MBDs at its N-terminal region, all of which are homologous. Since Hah1 can form two complexes of different geometries with MBD4, it raises the possibility of Hah1 interacting with two MBDs simultaneously, in which each interaction mode resembles one geometry. Cooperative effects among WDP MBDs might then exist in interaction with Hah1, facilitating Cu^{1+} transfer. Subsequently, the interactions of Hah1 with different combinations of WDP MBDs could play a role in the functional differences among the WDP MBDs.

4 Remaining challenges

The importance of metal homeostasis for cell function is becoming increasingly recognized. Intensive research is ongoing that employs a variety of experimental methods to elucidate the structures, dynamics, and functions of molecular players. In this article we summarized our recent contributions in using single-molecule fluorescence methods to understand the functions of metalloregulators and metallochaperones. Many insights can be learned, some of which are often unavailable or difficult to obtain from ensemble-averaged measurements. Still, many compelling questions remain. Here we discuss briefly some of the remaining challenges from our perspective.

4.1 Metalloregulators

For MerR-family metalloregulators, the actions of the protein on the DNA dictate the transcription suppression or activation. The small magnitude of the protein-induced DNA structural changes makes them difficult to study. By using engineered DNA HJs as reporters in smFRET measurements, we have been able to detect the protein-induced DNA-bending motion and examine the dynamics of protein–DNA interactions. Besides DNA-bending, the slight unwinding ($\sim 30^\circ$) of DNA by the holo-protein is essential for transcriptional activation as described in the DNA-distortion mechanism,^{35,37,38} and we have not detected DNA unwinding using the current design of engineered HJs. We are pursuing different design strategies of engineered HJs to target this DNA unwinding by MerR-family metalloregulators.

The DNA junction in a HJ also introduces concerns about the perturbation of the junction structure and the presence of the other helix on the protein–DNA interactions. Indeed, we have observed a weaker binding affinity of the metalloregulator to conf-I of the HJ, as compared with that to a double-strand DNA. Nevertheless, using HJs as reporters might have physiological relevance. If DNA recombination, which produces a HJ structure, occurs at the promoter region of a gene, studies of metalloregulator–HJ interactions can provide fundamental knowledge about how gene transcription is likely regulated or affected during this process.

As discussed in Section 2.3, the stronger DNA binding affinity of holo-metalloregulators than that of apo-metalloregulators raises implications about how transcription is turned off after activation. To return to the suppressed state, direct dissociation of

the holo-metalloregulator from DNA followed by binding of apo-metalloregulator is a possible scenario. Although we can estimate on the protein binding/unbinding kinetics from our current studies, quantitative information is not yet available. By labeling the protein with a FRET acceptor and the DNA with a donor, their binding/unbinding kinetics can be monitored directly. Research along this line is currently underway in our group.

4.2 Metallochaperones

Using nanovesicle trapping and smFRET, we have been able to follow the weak and dynamic Hah1–MBD4 interactions in real time, identifying multiple interaction complexes and quantifying their interaction kinetics. But, between the two complexes, which complex is productive for Cu^{1+} transfer, or are both productive? To address this question, observing Cu^{1+} transfer directly during protein interaction would be the best. But it is challenging to do because the d^{10} electron configuration of Cu^{1+} makes it magnetically silent and optically invisible, except for X-ray-based techniques. Our smFRET measurements cannot directly observe Cu^{1+} transfer, either. Nonetheless, as we are able to study the protein interactions in real time and quantitatively, we can study the perturbations of Cu^{1+} on the Hah1–MBD4 interaction dynamics. Significant changes in the Hah1–MBD4 interactions have been observed in the presence of Cu^{1+} in the solution (unpublished results). Although indirect, the Cu^{1+} -dependent Hah1–MBD4 interaction dynamics should provide information on how the dynamic protein interactions are coupled to the metal transfer process. Perturbations of the protein interactions by other metal ions, such as Hg^{2+} or Ag^{1+} , can also be studied; possible differences or similarities in comparison with those of Cu^{1+} can inform on the effect of metal–ligand bond strength on the protein interaction dynamics and possibly metal transfer.

WDP contains six MBDs in the N-terminal soluble region, many of which can interact with Hah1 for Cu^{1+} transfer. Whether and how these MBDs affect one another in their interactions with Hah1 is unclear. Our observation that Hah1 can form multiple complexes with a single WDP MBD raises the possibility that Hah1 can interact with multiple MBDs simultaneously, in which cooperative effects among MBDs could exist. Using nanovesicle trapping and smFRET, Hah1 interaction with multi-domain WDP constructs as well as interactions between different WDP MBDs can be also studied. The FRET probes can also be attached to various locations on the proteins to map the protein interaction geometries in detail. Three-color FRET can further be used to monitor two inter-distances simultaneously,⁸² so cooperative motions can be probed directly. With all the possible single-molecule tools, we expect more insights will emerge.

5 Acknowledgements

We thank our collaborators Profs. Chuan He, David L. Huffman, and Amy C. Rosenzweig for their contributions to the research described in this article. We also thank the National Institute of Health (GM082939), National Science Foundation (CHE0645392), Camille and Henry Dreyfus New Faculty Award, and Alfred F. Sloan Research Fellowship for funding our research. J.J.B. and A.M.K. were partially supported by National Institute of Health Molecular Biophysics Traineeships.

6 References

- 1 S. J. Lippard and J. M. Berg, *Principles of Bioinorganic Chemistry*, University Science Books, Mill Valley, 1994.
- 2 K. J. Waldron, J. C. Rutherford, D. Ford and N. J. Robinson, *Nature*, 2009, **460**, 823–830.
- 3 S. C. Andrews, A. K. Robinson and F. Rodriguez-Quinones, *FEMS Microbiol. Rev.*, 2003, **27**, 215–237.
- 4 L. A. Finney and T. V. O'Halloran, *Science*, 2003, **300**, 931–936.
- 5 N. C. Andrews, *Curr. Opin. Chem. Biol.*, 2002, **6**, 181–186.
- 6 D. H. Nies, *FEMS Microbiol. Rev.*, 2003, **27**, 313–339.
- 7 T. V. O'Halloran, *Science*, 1993, **261**, 715–725.
- 8 D. P. Giedroc and A. I. Arunkumar, *Dalton Trans.*, 2007, 3107–3120.
- 9 T. V. O'Halloran and V. C. Culotta, *J. Biol. Chem.*, 2000, **275**, 25057–25060.
- 10 A. C. Rosenzweig, *Acc. Chem. Res.*, 2001, **34**, 119–128.
- 11 P. S. Donnelly, Z. Xiao and A. G. Wedd, *Curr. Opin. Chem. Biol.*, 2007, **11**, 128–133.
- 12 P. A. Cobine, F. Pierrel and D. R. Winge, *Biochim. Biophys. Acta, Mol. Cell Res.*, 2006, **1763**, 759–772.
- 13 W. E. Moerner and D. P. Fromm, *Rev. Sci. Instrum.*, 2003, **74**, 3597–3619.
- 14 X. Michalet, S. Weiss and M. Jaeger, *Chem. Rev.*, 2006, **106**, 1785–1813.
- 15 T. Ha, *Methods*, 2001, **25**, 78–86.
- 16 X. Zhuang, *Annu. Rev. Biophys. Biomol. Struct.*, 2005, **34**, 399–414.
- 17 P. Chen and N. M. Andoy, *Inorg. Chim. Acta*, 2008, **361**, 809–819.
- 18 S. K. Sarkar, N. M. Andoy, J. J. Benitez, P. R. Chen, J. S. Kong, C. He and P. Chen, *J. Am. Chem. Soc.*, 2007, **129**, 12461–12467.
- 19 N. M. Andoy, S. K. Sarkar, Q. Wang, D. Panda, J. J. Benitez, A. Kalininskiy and P. Chen, *Biophys. J.*, 2009, **97**, 844–852.
- 20 J. J. Benitez, A. M. Keller, P. Ochieng, L. A. Yatsunyk, D. L. Huffman, A. C. Rosenzweig and P. Chen, *J. Am. Chem. Soc.*, 2008, **130**, 2446–2447.
- 21 J. J. Benitez, A. M. Keller, P. Ochieng, L. A. Yatsunyk, D. L. Huffman, A. C. Rosenzweig and P. Chen, *J. Am. Chem. Soc.*, 2009, **131**, 871.
- 22 J. J. Benitez, A. M. Keller and P. Chen, *Methods Enzymol.*, 2009, accepted.
- 23 T. Barkey, S. M. Miler and A. O. Summers, *FEMS Microbiol. Rev.*, 2003, **27**, 355–384.
- 24 N. L. Brown, J. V. Stoyanov, S. P. Kidd and J. L. Hobman, *FEMS Microbiol. Rev.*, 2003, **27**, 145–163.
- 25 L. Busenlehner, M. A. Pennella and D. P. Giedroc, *FEMS Microbiol. Rev.*, 2003, **27**, 131–143.
- 26 J. S. Cavet, G. P. M. Borrelly and N. J. Robinson, *FEMS Microbiol. Rev.*, 2003, **27**, 165–181.
- 27 M. Mergeay, S. Monchy, T. Vallaey, V. Auquier, A. Benotmane, P. Bertin, S. Taghavi, J. Dunn, D. van der Lelie and R. Wattiez, *FEMS Microbiol. Rev.*, 2003, **27**, 385–410.
- 28 C. Rensing and G. Grass, *FEMS Microbiol. Rev.*, 2003, **27**, 197–213.
- 29 M. Solioz and J. V. Stoyanov, *FEMS Microbiol. Rev.*, 2003, **27**, 183–195.
- 30 D. G. Kehres and M. E. Maguire, *FEMS Microbiol. Rev.*, 2003, **27**, 263–290.
- 31 J. R. Lloyd, *FEMS Microbiol. Rev.*, 2003, **27**, 411–425.
- 32 S. B. Mulrooney and R. P. Hausinger, *FEMS Microbiol. Rev.*, 2003, **27**, 239–261.
- 33 J. L. Hobman, J. Wilkie and N. L. Brown, *BioMetals*, 2005, **18**, 429–436.
- 34 T. V. O'Halloran, B. Frantz, M. K. Shin, D. M. Ralston and J. G. Wright, *Cell*, 1989, **56**, 119–129.
- 35 B. Frantz and T. V. O'Halloran, *Biochemistry*, 1990, **29**, 4747–4751.
- 36 P. R. Chen and C. He, *Curr. Opin. Chem. Biol.*, 2008, **12**, 214–221.
- 37 E. E. Zheleznova and R. G. Brennan, *Nature*, 2001, **409**, 378–382.
- 38 K. J. Newberry and R. G. Brennan, *J. Biol. Chem.*, 2004, **279**, 20356–20362.
- 39 S. Weiss, *Nat. Struct. Biol.*, 2000, **7**, 724–729.
- 40 D. M. J. Lilley, *Q. Rev. Biophys.*, 2000, **33**, 109–159.
- 41 S. A. McKinney, A. C. Declais, D. M. J. Lilley and T. Ha, *Nat. Struct. Biol.*, 2003, **10**, 93–97.
- 42 K. Mizuuchi, *Annu. Rev. Biochem.*, 1992, **61**, 1011–1051.
- 43 B. F. Eichman, J. M. Vargason, B. H. M. Mooers and P. S. Ho, *Proc. Natl. Acad. Sci. U. S. A.*, 2000, **97**, 3971–3976.
- 44 M. Ortiz-Lombardia, A. González, R. Eritja, J. Aymami, F. Azorín and M. Coll, *Nat. Struct. Biol.*, 1999, **6**, 913–917.
- 45 M. A. Karymov, M. Chinnaraj, A. Bogdanov, A. R. Srinivasan, G. Zheng, W. K. Olson and Y. L. Lyubchenko, *Biophys. J.*, 2008, **95**, 4372–4383.
- 46 A. Heltzel, I. W. Lee, P. A. Totis and A. O. Summers, *Biochemistry*, 1990, **29**, 9572–9584.
- 47 D. L. Huffman and T. V. O'Halloran, *Annu. Rev. Biochem.*, 2001, **70**, 677–701.
- 48 L. Banci and A. Rosato, *Acc. Chem. Res.*, 2003, **36**, 215–221.
- 49 P. C. Bull, G. R. Thomas, J. M. Rommens, J. R. Forbes and D. W. Cox, *Nat. Genet.*, 1993, **5**, 327–337.
- 50 I. Hamza, M. Schaefer, L. W. J. Klomp and J. D. Gitlin, *Proc. Natl. Acad. Sci. U. S. A.*, 1999, **96**, 13363–13368.
- 51 D. Larin, C. Mekios, K. Das, B. Ross, A.-S. Yang and T. C. Gilliam, *J. Biol. Chem.*, 1999, **274**, 28497–28504.
- 52 J. M. Walker, R. Tsivkovskii and S. Lutsenko, *J. Biol. Chem.*, 2002, **277**, 27953–27959.
- 53 L. Banci, I. Bertini, F. Cantini, C. Massagni, M. Migliardi and A. Rosato, *J. Biol. Chem.*, 2009, **284**, 9354–9360.
- 54 S. Lutsenko, K. Petrukhin, M. J. Cooper, T. C. Gilliam and J. H. Kaplan, *J. Biol. Chem.*, 1997, **272**, 18939–18944.
- 55 R. A. Pufahl, C. P. Singer, K. L. Peariso, S.-J. Lin, P. J. Schmidt, C. J. Fahrni, V. C. Culotta, J. E. Penner-Hahn and T. V. O'Halloran, *Science*, 1997, **278**, 853–856.
- 56 A. K. Wernimont, D. L. Huffman, A. L. Lamb, T. V. O'Halloran and A. C. Rosenzweig, *Nat. Struct. Biol.*, 2000, **7**, 766–771.
- 57 F. Arnesano, L. Banci, I. Bertini and M. J. J. Bonvin, *Structure*, 2004, **12**, 669–676.
- 58 L. Banci, I. Bertini, F. Cantini, C. T. Chasapis, N. Hadjiladis and A. Rosato, *J. Biol. Chem.*, 2005, **280**, 38259–38263.
- 59 D. Achila, L. Banci, I. Bertini, J. Bunce, S. Ciofi-Baffoni and D. L. Huffman, *Proc. Natl. Acad. Sci. U. S. A.*, 2006, **103**, 5729–5734.
- 60 D. Huster and S. Lutsenko, *J. Biol. Chem.*, 2003, **278**, 32212–32218.
- 61 S. Lutsenko, E. S. LeShane and U. Shinde, *Arch. Biochem. Biophys.*, 2007, **463**, 134–148.
- 62 J. M. Walker, D. Huster, M. Ralle, C. T. Morgan, N. J. Blackburn and S. Lutsenko, *J. Biol. Chem.*, 2004, **279**, 15376–15384.
- 63 L. A. Yatsunyk and A. C. Rosenzweig, *J. Biol. Chem.*, 2007, **282**, 8622–8631.
- 64 E. M. W. M. van Dongen, L. W. J. Klomp and M. Merckx, *Biochem. Biophys. Res. Commun.*, 2004, **323**, 789–795.
- 65 D. L. Huffman and T. V. O'Halloran, *J. Biol. Chem.*, 2000, **275**, 18611–18614.
- 66 G. Multhaup, D. Strausak, K.-D. Bissig and M. Solioz, *Biochem. Biophys. Res. Commun.*, 2001, **288**, 172–177.
- 67 D. Strausak, M. K. Howies, S. D. Firth, A. Schlicksupp, R. Pipkorn, G. Multhaup and J. F. B. Mercer, *J. Biol. Chem.*, 2003, **278**, 20821–20827.
- 68 F. Arnesano, L. Banci, I. Bertini, F. Cantini, S. Ciofi-Baffoni, D. L. Huffman and T. V. O'Halloran, *J. Biol. Chem.*, 2001, **276**, 41365–41376.
- 69 L. Banci, I. Bertini, F. Cantini, N. Della-Malva, M. Migliardi and A. Rosato, *J. Biol. Chem.*, 2007.
- 70 L. Banci, I. Bertini, C. Francesca, A. C. Rosenzweig and L. A. Yatsunyk, *Biochemistry*, 2008, **47**, 7423–7429.
- 71 D. T. Chiu, C. F. Wilson, A. Karlsson, A. Danielsson, A. Lundqvist, A. Strömberg, F. Ryttsén, M. Davidson, S. Nordholm, O. Orwar and R. N. Zare, *Chem. Phys.*, 1999, **247**, 133–139.
- 72 E. Boukobza, A. Sonnenfeld and G. Haran, *J. Phys. Chem. B*, 2001, **105**, 12165–12170.
- 73 E. Rhoades, E. Gussakovsky and G. Haran, *Proc. Natl. Acad. Sci. U. S. A.*, 2003, **100**, 3197–3202.
- 74 G. Haran, *J. Phys.: Condens. Matter*, 2003, **15**, R1291–R1317.
- 75 E. Rhoades, M. Cohen, B. Schuler and G. Haran, *J. Am. Chem. Soc.*, 2004, **126**, 14686–14687.
- 76 B. Okumus, T. J. Wilson, D. M. J. Lilley and T. Ha, *Biophys. J.*, 2004, **87**, 2798–2806.
- 77 J. Y. Lee, B. Okumus, D. S. Kim and T. Ha, *Proc. Natl. Acad. Sci. U. S. A.*, 2005, **102**, 18938–18943.
- 78 I. Cisse, B. Okumus, C. Joo and T. Ha, *Proc. Natl. Acad. Sci. U. S. A.*, 2007, **104**, 12646–12650.
- 79 B. Okumus, S. Arslan, S. M. Fengler, S. Myong and T. Ha, *J. Am. Chem. Soc.*, 2009, **131**, 14844–14849.
- 80 I. Anastassopoulou, L. Banci, I. Bertini, F. Cantini, E. Katsari and A. Rosato, *Biochemistry*, 2004, **43**, 13046–13053.
- 81 *Protein-Protein Recognition*, ed. C. Kleantous, Oxford University Press, Oxford, 2000.
- 82 S. Hohng, C. Joo and T. Ha, *Biophys. J.*, 2004, **87**, 1328–1337.